Why Galaxies Care About AGB Stars:
A Continuing Challenge through Cosmic Time
Proceedings IAU Symposium No. 343, 2019
F. Kerschbaum, M. Groenewegen & H. Olofsson, eds.

doi:10.1017/S1743921319001819

Planetary Nebulae, Morphology and Binarity, and the relevance to AGB Stars

Raghvendra Sahai

Jet Propulsion Laboratory MS 183-900, California Institue of Technology,
Pasadena, CA 91109, USA
email: raghvendra.sahai@jpl.nasa.gov

Abstract. The dramatic transformation of the spherical outflows of AGB stars into the extreme aspherical geometries seen during the planetary nebula (PN) phase is widely believed to be linked to binarity and is likely driven by the associated production of fast jets and central disks/torii. We first briefly summarize results from the imaging surveys of large samples of young PNe and pre-PNe with HST which show that almost all objects have bipolar, multipolar and elliptical morphologies, with widespread presence of point-symmetric structure. We describe a relatively new technique of using UV photometic observations of large AGB star samples to search for binarity and associated accretion activity, and follow-up studies using UV spectroscopy and X-ray observations. We present results from studies of individual objects in transition to the PN phase, highlighting observational techniques being used to determine jet properties that can constrain the accretion modes that power these jets.

Keywords. stars: AGB and post-AGB, instrumentation: High angular resolution, ISM: planetary nebulae:general

1. Introduction

Most stars in the Universe that evolve in a Hubble time (i.e., those with main-sequence masses 1-8$M_{\odot}$) die extraordinary deaths, ejecting half or more of their total mass in the form of nucleosynthetically-enriched material into the interstellar medium (ISM) – a process which dramatically alters the course of stellar evolution, and plays a key role in the chemical evolution of galaxies. The death throes of these stars enrich the ISM in biogenically important elements like C and N, and sow the seeds for the birth of new stars and solar systems, yet this stage remains very poorly understood. Young planetary nebulae (YPNe) represent the bright end-stages of these stars and provide valuable diagnostics on their demise, however, PN formation, and the phase of extreme mass-loss at end of the asymptotic red giant (AGB) phase that leads to it, is very poorly understood. Most YPNe have bipolar or multipolar shapes and very few are round, and more than half of all PNe show collimated lobes and dense, dusty, equatorial waists, which are important morphological features of this class of objects (e.g., Sahai & Trauger 1998 [ST98], Sahai *et al.* 2011a [SMV11]). Binarity is widely believed to be the (likely) underlying cause for the dramatic AGB-to-PN transition, e.g, directly via common-envelope ejection (Ivanova *et al.* 2013) and/or accretion-disk and torus formation, or indirectly via increased rotation and the generation of strong magnetic fields (e.g., Soker 2015, De Marco 2009, Chamandy *et al.* 2018, Jones 2018).

Three morphologically-unbiased HST imaging surveys have observationally bracketed the evolutionary phases that span the spherical to aspherical transition. These surveys imaged (1) YPNe (i.e., compact, with size <5–10 arcseconds, and the flux ratio [OIII]/H$\alpha \lesssim 1$) (ST98, SMV11), (2) Pre-Planetary Nebulae or PPNe (IRAS 25-to-12μm

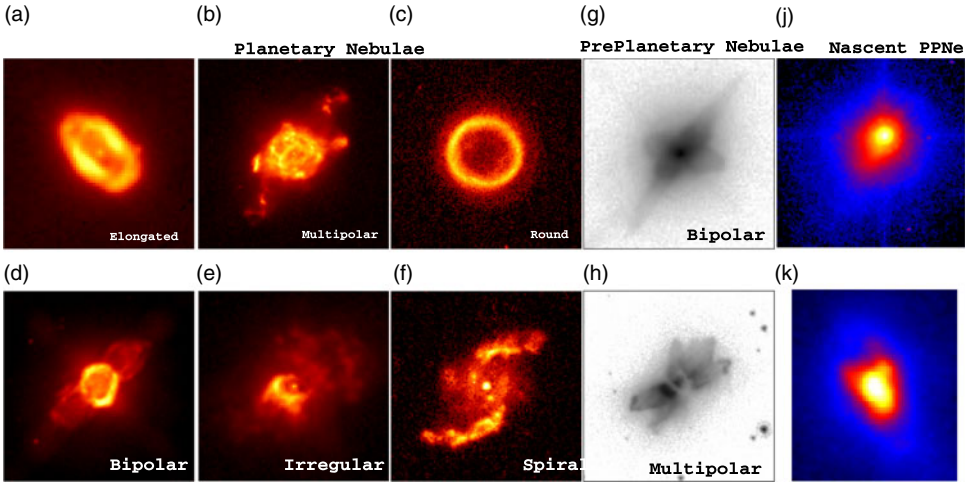

Figure 1. YPNe, PPNe and nascent-PPNe images from HST – (*a–f*) Hα (or [NII]) images of PNe belonging to 6 primary classes in the Sahai, Morris & Villar (2011) classification system, which consists of 7 primary classes based on the overall nebular shape, and several categories of secondary characteristics related to specific properties of the lobes, waist, and haloes, and the presence of point-symmetry; (*g,h*) 0.6 μm images of PPNe belonging to 2 primary classes; and (*j,k*) 0.6 μm images of nascent PPNe. (a) PNG 014.3 − 05.5 ($4\farcs0 \times 4\farcs0$), (b) PNG 027.6 − 09.6 ($11\farcs4 \times 11\farcs4$, (c) PNG 357.2 + 02.0 ($2\farcs67 \times 2\farcs67$), (d) PNG 356.5 − 03.9 ($6\farcs84 \times 6\farcs84$, (e) PNG 068.3 − 02.7 ($3\farcs8 \times 3\farcs8$), (f) PNG 032.1 + 07.0 ($4\farcs67 \times 4\farcs67$), (g) IRAS 04296+3429 ($3\farcs7 \times 3\farcs7$), (h) IRAS 19024+0044 ($6\farcs3 \times 6\farcs3$), (j) IRAS 23320+4316 ($0\farcs48 \times 0\farcs48$), & (k) IRAS 15082-4808 ($0\farcs69 \times 0\farcs8$).

flux ratio $F_{25}/F_{12} > 1.4$, to select for objects lacking warm dust, as an indicator that dense AGB mass loss has stopped recently) (Sahai *et al.* 2007), and (3) Nascent PPNe ($1 < F_{25}/F_{12} < 1.4$, to select for objects lacking hot dust, as an indicator that dense AGB mass loss is on the wane) (Sahai 2009). The PPN survey led to a systematic characterization scheme for the observed morphologies with 4 primary classes (B: bipolar, M: multipolar, E: elongated, and I: irregular) (e.g., Fig. 1(g,h)), and a number of secondary descriptors, relating to, e.g., the presence of point-symmetry, ansae, halos, etc. But the survey did not find a single round object.

The scheme was adapted to the morphological classification of YPNe, by adding 3 new primary classes – L (collimated lobe pair, but not pinched-in at the waist), R (round), and S (spiral arm), and additional secondary descriptors (SMV11, and Fig. 1(a-f)). Many of these secondary descriptors are related to features arising from evolutionary effects on the central region, due to (i) the ionizing flux and (ii) hydrodynamic action of the fast radiative wind from the PNe central star on this region. In contrast, the morphologies seen during the nascent PPN phase, based on our HST imaging survey, are rather different, with compact ($\lesssim few \times 0.1''$), one-sided collimated structures being predominant, suggesting that the collimated-outflow phase has just begun (Fig. 1(j,k), Sahai 2009).

The YPN survey led to the hypothesis that PN formation is preceded by the generation of collimated, high-speed outflows that sculpt the progenitor AGB envelope from the inside out, during the very late-AGB or nascent PPN phase (ST98). This hypothesis is supported by molecular line observations of PPNe that directly show the presence of collimated, high-speed outflows morphology (e.g., Bujurrabal *et al.* 2001, Sahai *et al.* 2006, Sánchez Contreras *et al.* 2006, Imai 2007, Sahai *et al.* 2017a; Sahai *et al.* 2017b). Binarity is widely believed to be the most probable cause for producing such outflows, which must start operating during the nascent PPN or late-AGB phase. But observational

https://doi.org/10.1017/S1743921319001819 Published online by Cambridge University Press

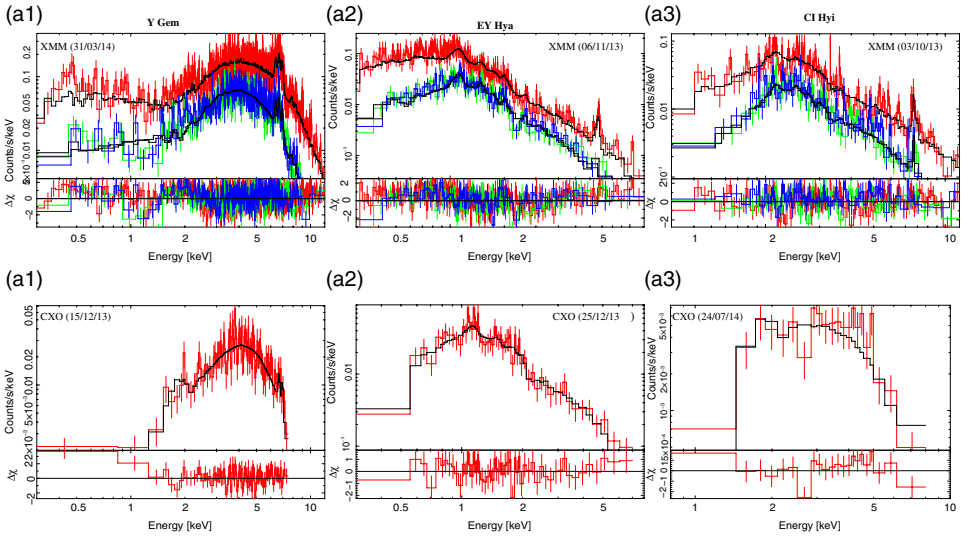

Figure 2. X-ray spectra for 3 fuvAGB stars, taken with (a) XMM/EPIC (pn: *red*, MOS1: *green*, MOS2: *blue*), and (b) CXO ACIS-S (red). APEC model fits are shown in *black*. APEC modeling of the CXO and XMM spectra reveals long-term variations in the emission properties (*adapted from Setal15*).

evidence for binarity and associated accretion-activity has generally been hard to come by. Standard methods for detecting binarity such as periodic radial-velocity or photospheric variations due to a companion cannot be used for AGB stars that are thousands of time more luminous than their expected companions and exhibit strong instrinsic atmospheric pulsations.

2. Binarity and Accretion Activity in AGB Stars

We developed an innovative technique of using UV observations to search for binarity and associated accretion activity – since most AGB stars are relatively cool ($T_{\rm eff} \lesssim 3000$K) objects (spectral types ∼M6 or later), whereas any (likely) stellar companions (i.e., white-dwarfs [WD] or main-sequence [MS]) and/or accretion disks around them are likely significantly hotter ($T_{\rm eff} \gtrsim 6000$K), favorable secondary-to-primary flux contrast ratios ($\gtrsim$10) are reached in the GALEX FUV (1344-1786Å) and NUV (1771-2831Å) bands for a source with $T_{\rm eff} \gtrsim$6000 K and luminosity, $L \gtrsim 1 L_{\odot}$ (companion and/or disk). The feasibility of this technique was demonstrated in a number of recent studies (Sahai *et al.* 2008 [Setal08]; Sahai *et al.* 2011b; Sahai *et al.* 2016a). Setal08 detected emission from 9/21 objects in the FUV; since such objects (hereafter fuvAGB stars) also show significant UV variability, Setal08 concluded that the UV source is unlikely to be solely a companion's photosphere, and is likely dominated by emission related to variable accretion activity. It should be noted that fuvAGB stars in general (based on their optical spectra), do not belong to the well-studied class of symbiotic stars (red giant stars with WD companions) and have never been classified as such. So if the compact companions in fuvAGB star systems are WDs, then these must be quite cool ($\lesssim 20\,000$ K) (Sahai *et al.* 2015 [Setal15]).

Our small X-rays surveys using XMM-Newton and Chandra support this hypothesis, finding X-ray emission in about 50% of the fuvAGB stars. The X-ray emission is characterised by relatively high luminosities $L_{\rm x} \sim (0.002 - 0.11)\, L_{\odot}$, and very high plasma temperatures $T_{\rm x} \sim (35 - 160) \times 10^6$ K (Setal15), Fig. 2. Amongst the fuvAGB stars, objects with large FUV/NUV ratios, $R_{\rm fuv/nuv} > 0.17$, have a much higher probability

https://doi.org/10.1017/S1743921319001819 Published online by Cambridge University Press

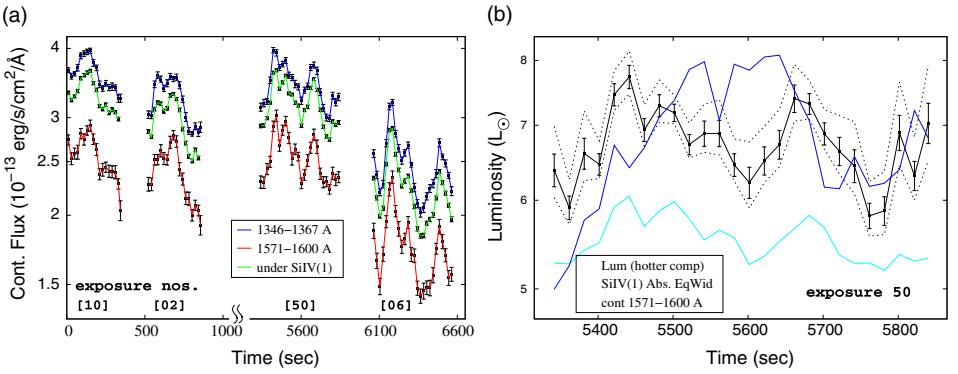

Figure 3. Short-term time variations in the (a) FUV continuum: line-free continuum in the bands 1346 − 1367 Å (blue) and 1571 − 1600 Å (red), and continuum underlying the Si IV(1) line (green), and (b) luminosity (black) of the high-temperature accretion component, derived using a two-blackbody fit to the continuum observed in the subexposures within exposure 50: the dashed curves show upper and lower bounds on the luminosity due to the estimated uncertainties in the cooler blackbody's luminosity and temperature. The 1571 − 1600 Å continuum, scaled up by a factor 1.1×10^7 (cyan), and the square-root of the Si IV(1) absorption line equivalent width, scaled up by a factor 5.2 (blue), are shown for comparison (*adapted from Setal18*).

of being detected in X-ray emission (Sahai *et al.* 2016a), and are almost certainly binaries with accretion activity powering the high-energy emission. A recent STIS spectroscopic study of the prototype high FUV/NUV ratio star, Y Gem, shows the presence of flickering and high-velocity infall and outflows, and thus directly supports the binary/accretion hypothesis (Sahai *et al.* 2018a [Setal18]). STIS observations of Y Gem show several UV lines from species such as Si IV and C IV, with broad (FWHM $\sim 300 - 700\,\mathrm{km\ s^{-1}}$) emission and absorption features that are red- and blue- shifted by velocities of $\sim$500 km s^{-1} from the systemic velocity. Time-tag analysis reveals strong flickering in the UV continuum on time-scales of $\lesssim 20$ s (Fig. 3a), characteristic of an active accretion disk. A two blackbody model that fits the G140L and G230L spectra requires two components, a hotter one with luminosity $L(h) = 6.8\,L_\odot$ and temperature $T_{\rm eff}(h) \sim 36600$ K, and a cooler blackbody with $L(c) \sim 6.3\,L_\odot$, $T_{\rm eff}(c) \sim 9940$ K; we find significant variations in $L(h)$ (Fig. 3b), but not in $T_{\rm eff}(h)$. Neither of these two blackbodies fit the properties of a viable stellar companion (WD or MS) to the primary, and it is likely that both the hot and cool UV components arise in the accretion disk.

The proposed model for these (and previous) observations is that material from the primary star is gravitationally captured by a companion, producing a hot accretion disk. The latter powers a fast outflow that produces blue-shifted features due to absorption of UV continuum emitted by the disk, whereas the red-shifted emission features arise in heated infalling material from the primary. The outflow velocities support a previous inference by Setal15 that Y Gem's companion is a low-mass MS star.

But for objects with little or no FUV emission, i.e., with $R_{\rm fuv/nuv} \lesssim 0.1$ (nuvAGB stars), which dominate the population of UV-emitting AGB stars, the UV emission *may have a different source*. From an analysis of the NUV emission in 179 AGB stars, Montez *et al.* (2017) argued that the origin of the GALEX-detected UV emission is intrinsic to the AGB star (chromospheric & photospheric emission), and is unrelated to binarity. However, Ortiz & Guerrero (2016), from a study of a volume-limited sample (<0.5 kpc) of 58 AGB stars, concluded that the detection of NUV emission with a very large observed-to-predicted ratio, $Q_{\rm NUV} > 20$, is evidence for binarity in these objects.

Thus a more comprehensive (and easily testable) hypothesis for UV emission from AGB stars is that objects with a close companion produce high FUV/NUV ratios at

https://doi.org/10.1017/S1743921319001819 Published online by Cambridge University Press

least some of the time (since accretion can be variable) and/or a very large NUV excess, whereas single AGB stars (or those with large binary separations) should always show low FUV/NUV ratios. UV spectroscopy provides an unambiguous and independent test of this hypothesis because accretion-related activity is expected to produce UV lines with large widths and large Doppler shifts (as shown by the study of Y Gem). In contrast, chromospheric emission typically arising from gas at temperatures of $\lesssim 10^4$ K (e.g., Luttermoser *et al.* 1994), should be characterised by strong low-excitation lines in the NUV (such as the MgII λ2800 doublet), with the high-excitation UV lines being much weaker or absent. In addition, chromospheric line profiles from the AGB star will be relatively narrow ($\lesssim$10 km s^{-1}) and close to the systemic velocity.

2.1. *Additional Probes of Accretion Activity*

Multi-wavelength radio observations can distinguish between thermal and non-thermal emission (Sahai 2018a): since binarity is also expected to generate strong magnetic fields, ionized accretion-related flows can produce non-thermal, variable, emission, as we have found for Y Gem. The VLA lacks the sensitivity to make such observations except for a few ($\lesssim 5$) of the brightest objects, but the ngVLA should be able to carry out a survey for a statistical sample of AGB stars (i.e., several 100) with UV emission with a modest time expenditure ($\sim$ 1 hr per object to cover 4 bands in the 8–90 GHz range with a 5 σ sensitivity of about 3.5 μJy) (Sahai 2018a).

We may be able to detect optical flickering with the TESS mission, with its extreme photometric accuracy – 1σ noise sensitivity of 690 (340) ppm in 2 min exposures for our faintest (median brightness) object – thus sensitive to fractional variations that are a factor 200 or larger below that in the FUV (peak-to-peak of 40%). We note that optical flickering has been detected by Snaid *et al.* (2018) in Y Gem (0.06 mag peak-to-peak in the u' band on typical timescales of $\sim$10 min).

3. Binarity and late-AGB & early post-AGB Evolution

Binary interactions can, directly or indirectly, produce dense waists and collimated fast outflows or jets (e.g., De Marco 2009, Kastner *et al.* 2012). Hydrodynamic sculpting by these jets of the superwind ejecta can then produce the variety of PN shapes observed (ST98). In order to assess this scenario for PN shaping, we need to understand the origin and properties of these jets (e.g., the associated mass, speeds, opening angles). We need to know whether the jets are episodic and if the jet axis precesses or wobbles, and if so, on what time-scales, and the role of magnetic fields in launching, accelerating and collimating the high-speed outflows. Unlike AGB outflows, for the small sample of PPNe outflows (with typical speeds of $\sim few \times 100$ km s^{-1}) studied so far, the associated momenta, as inferred from an analysis of (mostly single-dish) CO and ^{13}CO line profiles in PPNe, are far too high for these to be driven radiatively (e.g., Bujurrabal *et al.* 2001). We also need to understand the origin and properties of equatorially-dense structures, i.e., the waists, and whether these are bound or expanding.

Quantitative models for the binary interaction that can explain the jet and waist formation are lacking, partly because simulations have long struggled to describe binary interactions, even in the simplest cases. However, Blackman & Lucchini (2014: BL14) show how the properties of the high-velocity flows in PPNe can be used to constrain jet-engine paradigms using an analytical modelling approach, and provide a classification of the interactions and their observational signatures, thus distinguishing the type of engines that eject mass via jet-like collimated outflows.

In order to address these questions, it is important to focus on the late-AGB, nascent-PPN and PPN phases. Some notable recent studies of AGB stars are that of L_2 Pup, revealing a dusty disk with Keplerian rotation, a low-mass candidate

https://doi.org/10.1017/S1743921319001819 Published online by Cambridge University Press

companion (giant planet or low-mass brown dwarf) using polarimetric imaging with the SPHERE+ZIMPOL instrument of the VLT and ALMA (Kervella *et al.* 2015, 2016) and π^1 Gru, revealing a flared disk using ALMA (Nhung *et al.* 2016). In this paper, I summarize results on three key objects that cover the nascent PPN, YPN and PPN phases.

3.1. *The Carbon Star V Hya: A Nascent PPN*

The carbon star, V Hya, is a key object in understanding the early transition of AGB stars into aspherical PNe, as it shows the presence of high-speed, collimated outflows and dense equatorial structures. This star is ejecting massive high-speed compact clumps (hereafter bullets) periodically, leading to a model in which the bullet ejection is associated with the periastron passage of a close binary companion in an eccentric orbit around V Hya with an orbital period of ∼8.5 yr (Sahai *et al.* 2016b, hereafter Setal16). The detailed physical properties of this ejection suggests that the companion approaches the primary very close to the latter's stellar envelope at every periastron passage, suggesting that V Hya is a good candidate where the binary interaction will result in a CE configuration. A hot, central disk-like structure of diameter 0.″6 (240 AU at V Hya's distance of 400 pc) expanding at a speed of $10-15\,\mathrm{km\ s^{-1}}$ was found earlier by Sahai *et al.* (2003), using HST STIS observations. High resolution (∼ 100 milliarcsecond) imaging of the central region of V Hya using the coronagraphic mode of the Gemini Planet Imager (GPI) in the 1 μm band shows a larger (size ∼ 250 AU), central dusty disk (see Sahai *et al.* 2018b, this volume). The bullet ejection activity has likely been ongoing for several hundered years, and has carved out a bipolar cavity; detailed modelling of the most recently ejected bullets suggests that these are being shepherded towards the overall symmetry axis, and entrain ambient circumstellar material, as a result of glancing encounters with the walls of this cavity (Scibelli *et al.* 2018). Recent hydrodynamical simulations of the evolution of these bullets show that they carry embedded toroidal magentic fields within them that keep them confined laterally (Huang & Sahai 2018), as was found for the bullet-like clumps in the jet of the young PN, He 2-90 (Lee & Sahai 2004).

3.2. *IRAS 16342-3814: A young PPN*

IRAS 16342-3814 (hereafter IRAS 16342) belongs to a class of young PPNe with unusually fast radial H_2O outflows with $V_{\rm exp} \gtrsim 50\,\mathrm{km\ s^{-1}}$ ("water-fountain" PPNe) showing that jet activity is extremely recent ($\lesssim$ 100 yr), and indicating that these objects have become PPNe fairly recently. As the best studied and nearest (∼2 kpc) example of this class, its morphology has been well-resolved with optical (HST) and near-infrared (Keck Adaptive Optics) imaging (Sahai *et al.* 1999, Sahai *et al.* 2005). Radio interferometry (VLA, VLBA) shows water masers spread over a range of radial velocities encompassing $270\,\mathrm{km\ s^{-1}}$ (Sahai *et al.* 1999, Claussen *et al.* 2009).

From an ALMA study in which emission from ^{12}CO J=3–2 and other molecular lines was mapped with ∼ 0.″35 resolution, Sahai *et al.* (2017a, hereafter Setal17) inferred the presence of two very high-speed, knotty, jet-like molecular outflows, and a central expanding torus. The outflows include the Extreme High Velocity Outflow (EHVO) and the High Velocity Outflow (HVO) with (deprojected) expansion speeds of $360-540$ and $250\,\mathrm{km\ s^{-1}}$ and ages of $130-305$ yr and $\lesssim 110$ yr; their axes are not colinear. The spiral structure seen in a position-velocity (PV) plot of the HVO most likely indicates emission from a precessing high-velocity bipolar outflow, as inferred previously from near-IR imaging (Sahai *et al.* 2005), that entrains material in the near and far bipolar lobe walls. The progenitor AGB star of IRAS 16342 underwent a sudden, very large increase (by a factor >500) in its mass-loss rate ∼455 yr ago, with an average value over this period

https://doi.org/10.1017/S1743921319001819 Published online by Cambridge University Press

of $> 3.5 \times 10^{-4}\, M_\odot$ yr^{-1}. The measured expansion ages of the outflows and torus imply that the torus (age$\sim$160 yr) and the younger high-velocity outflow (age$\sim$110 yr) were formed soon after the sharp increase in the AGB mass-loss rate.

3.3. *The Boomerang Nebula: A post-RGB PPN*

The Boomerang Nebula, is an "extreme" bipolar pre-planetary Nebula (PPN), and also the coldest known object in the Universe, with a massive high-speed outflow that has cooled significantly below the cosmic background temperature (Sahai & Nyman 1997). ALMA observations have confirmed this finding, revealed unseen distant regions of this ultra-cold outflow (UCO) out to $\gtrsim 120\,000$ AU, and found that the expansion velocity in the UCO is not constant, but increases with radius (Sahai *et al.* 2013, Sahai *et al.* 2017b). The very large mass-loss rate ($\sim 0.001\, M_\odot$ yr^{-1}) characterising the UCO and the central star's very low-luminosity ($300\, L_\odot$) are unprecedented, making it a key object for testing theoretical models for mass-loss during post-main sequence evolution and for producing the dazzling variety of bipolar and multipolar morphologies seen in PNe (e.g., SMV11). The mass-loss rate ($\dot{M}$) increases with radius in the UCO, similar to its expansion velocity (V) – taking $V \propto r$, Sahai *et al.* (2017b) find $\dot{M} \propto r^{0.9-2.2}$. The mass in the UCO is $\gtrsim 3.3\, M_\odot$, and the Boomerang's MS progenitor mass is $\gtrsim 4\, M_\odot$. The UCO's kinetic energy is very high, $KE_{\rm UCO} > 4.8 \times 10^{47}$ erg, and the most likely source of this energy is the gravitational energy released via binary interaction in a common envelope event (CEE). Sahai *et al.* (2017b) concluded that the Boomerang's primary was an RGB or early-AGB star when it entered the CE phase; the companion finally merged into the primary's core, ejecting the primary's envelope that now forms the UCO. Such strong binary interactions on the RGB may in fact be a common evolutionary channel, given that Kamath *et al.* (2015, 2016) have recently identified a large sample of post-RGB objects in the Large and Small Magellanic Clouds. Many PPNe in our Galaxy, for which distances are not known, may really be post-RGB objects!

4. Accretion Modes

The objects discussed above show evidence for episodic, collimated jet-like outflows, but with significant differences. The accuracy of BL14's analysis (see § 3) depends on how well we can determine the physical properties of the fast outflows in PPNe (especially the jet momentum, $M_{\rm j}\, V_{\rm j}$, and the accretion time-scale, $t_{\rm acc}$), and the history of the progenitor AGB's mass-loss in the last $\sim 100 - 1000$ yr. Using the limited outflow data known to date at "face-value", BL14 determine the minimum required mass-accretion rates ($\dot{M}_{\rm a} \propto M_{\rm j}\, V_{\rm j}/t_{\rm acc}$) and rule out some accretion modes such as Bondi-Hoyle-Lyttleton (BHL) wind-accretion and wind Roche lobe overflow (wRLOF). In BL14's approach, the intrinsic jet momentum is estimated from the observed fast outflow's momentum, assuming that the interaction between the intrinsic jet outflow and the ambient circumstellar envelope is momentum-conserving.

In Y Gem, Setal18 conclude, from their UV spectroscopic study, that material from the primary star is gravitationally captured by a low-mass MS companion producing a hot accretion disk around the latter. The disk powers a fast outflow that produces blue-shifted features due to absorption of UV continuum emitted by the disk, whereas the red-shifted emission features arise in heated infalling material from the primary. The accretion luminosity implies a mass-accretion rate $> 5 \times 10^{-7}\, M_\odot$ yr^{-1}; Setal18 conclude that Roche lobe overflow is the most likely binary accretion mode since Y Gem does not show the presence of a wind.

https://doi.org/10.1017/S1743921319001819 Published online by Cambridge University Press

In V Hya, the collimated ejection of material is in the form of bullets, and the ejection axis flip-flops around an average orientation, in a regular manner. These data support a model in which the bullets are a result of collimated ejection from an accretion disk (produced by gravitational capture of material from the primary) that is warped and precessing, and/or that has a magnetic field that is misaligned with that of the companion or the primary star (Setal16). The average momentum rate of the bullet ejections is ($\sim 8.2 \times 10^{25}\,\mathrm{g\,cm\,s^{-2}}$), implying a minimum required accretion rate of $\dot{M}_{\rm a} \sim 3.3 \times 10^{-8}\,M_\odot\ \mathrm{yr}^{-1}$. Since the secondary must get very close to the primary's stellar envelope at periastron passage (Setal16), the binary separation is comparable to the stellar radius (at 400 pc, $R_* \sim 2\,\mathrm{AU}$: Knapp *et al.* 1997), i.e., $a_{\rm or} \sim 2\,\mathrm{AU}$, so the Roche-lobe overflow mode (RLOF) is the appropriate accretion mode, which can easily supply the required accretion rate.

In IRAS 16342, the relatively high momentum rate for the dominant jet-outflow ($> 5 \times 10^{28}\,\mathrm{g\,cm\,s^{-2}}$) implies a high minimum accretion rate, $\dot{M}_{\rm a} = 1.9 \times 10^{-5}\,M_\odot\ \mathrm{yr}^{-1}$. Comparing this rate with the expected mass-accretion rates derived for different accretion models shown in BL14's Fig. 1, Setal17 concluded that standard Bondi-Hoyle-Lyttleton (BHL) wind-accretion and wind-RLOF models with WD or MS companions were unlikely; enhanced RLOF from the primary or accretion modes operating within common envelope evolution were needed. But this conclusion was revised by Sahai (2018b) because the BHL rate shown in BL14's Fig. 1b is derived using the primary's AGB mass-loss properties $\dot{M}_{\rm w} = 10^{-5}\,M_\odot\ \mathrm{yr}^{-1}$ (and $V_{\rm w} = 10\,\mathrm{km\ s^{-1}}$, together with assumed orbital separation $a_{\rm or} = 10\,\mathrm{AU}$, companion mass $M_{\rm c} = 0.6\,M_\odot$, primary mass $M_{\rm p} = 1.0\,M_\odot$) and not the much higher value of $\dot{M} \sim 1.3 \times 10^{-4}\,M_\odot\ \mathrm{yr}^{-1}$ (comparable to the mass-loss rate in IRAS 16342), mentioned in BL14's § 3.1 and referenced in the figure caption (E. Blackman, *priv. comm.*). Thus, the expected BHL accretion rate could be quite high in IRAS 16342. However, Sahai (2018b) show that the BHL accretion rate, which is valid when the orbital separation is much larger than the Roche-lobe radius, is $\dot{M}_{\rm BHL} \lesssim (0.3-1) \times 10^{-5}\,M_\odot\ \mathrm{yr}^{-1}$, and therefore the HVO in IRAS 16342 is not driven by accretion via BHL, but requires wind-RLOF or modes that provide higher accretion rates.

The Boomerang's central region has an overall bipolar structure, but in detail this structure is comprised of multiple, highly collimated lobes on each side of the central disk, both in scattered light and in ^{13}CO J=3–2 emission. The velocity of the molecular material in the dense walls of the collimated lobes is not particularly high, and we expect it is likely to be substantially lower than the velocity of the unshocked jet-outflow that has carved out these lobes, since the jet outflow has interacted with a very massive envelope (the UCO). Optical spectroscopy, indicating that the pristine fast outflow may have a speed of about $100\,\mathrm{km\ s^{-1}}$ (Neckel *et al.* 1987), support this expectation. Assuming momentum-conservation to derive the fast outflow momentum (as in BL14) is likely to provide a severe underestimate of the intrinsic jet momentum – numerical simulations are needed. However, in this object, the UCO's extreme properties directly imply CE evolution.

5. Summary

(1) Binarity and associated accretion-activity on the AGB is best studied using observations at UV and X-Ray wavelengths, as demonstrated by our pilot studies. A focussed UV spectroscopic study of the prime example of this phenomenon, Y Gem, shows high speed outflow and infall, and the presence of a hot accretion disk. But more extensive surveys are now needed in order to determine whether binarity and accretion-activity are ubiquitous and to understand these phenomena in detail. An HST UV spectroscopic survey of AGB stars with high and low FUV/NUV ratios is needed to study the relative

https://doi.org/10.1017/S1743921319001819 Published online by Cambridge University Press

contributions to the UV due to accretion-activity, which would result from binarity, as opposed to chromspheric/coronal emission from a single star.
(2) The effects of binary interactions on post-AGB evolution is best studied using high-angular-resolution imaging & spectroscopic studies. An ALMA survey of PPNe covering the variety of morphologies seen in these objects is now needed in order to determine jet momenta and AGB mass-loss rates just prior to the post-AGB phase accurately, as well as to determine the nature of central disks/torii (when these are present). The nature and origin of these central disks/torii remains a mystery. Focussed studies of three objects in this transition phase have provided new details, leading to new insights:
(a) Our HST studies of V Hya implies the presence of a companion in an eccentric orbit, with a strong interaction at periastron passage leading to a stream of episodic, high-speed bullet-like ejections. Resonant precession of the disk/jet-axis as inferred for V Hya may explain the presence of multipolar morphologies, whereas non-resonant precession of disk/jet-axis can explain bipolar nebulae with point-symmetric knots. The bullets likely have an embedded toroidal magnetic field, that keeps them confined laterally.
(b) Our ALMA study of the young PPN IRAS 16342 shows two highly collimated, episodic, high-speed outflows which have different orientations, an expanding torus, and a large, sudden increase in AGB mass-loss rate over the past 500 years. Although such a high mass-loss rates potentially allows BHL accretion to power the dominant high-velocity outflow in this object, the wind-RLOF mode or modes that provide higher accretion rates are required for IRAS 16342. Our IRAS 16342 study underscores the importance of measuring AGB mass-loss rates immediately prior to the post-AGB phase.
(c) Our ALMA studies of the PPN, the Boomerang Nebula (also the coldest object in the Universe) show that it is a post-RGB object, resulting from a strong binary interaction on the RGB that ejected its envelope. It is thus possible that many low-luminosity PPNe may be post-RGB rather than post-AGB objects.

Acknowledgements

I thank Eric Blackman for a helpful discussion related to binary acretion modes. I thank my collaborators in the studies that have contributed to this paper, including C. Sánchez Contreras, J. Sanz-Forcada, W. Vlemmings, M. Morris, M. Claussen, J. Sanz-Forcada, L-Å. Nyman, and S. Scibelli. Special thanks to Orsola de Marco and Noam Soker for their quick responses to my questions related to binary evolution. The author's research described here was carried out at the Jet Propulsion Laboratory, California Institute of Technology, under a contract with NASA, and funded in part by NASA via ADAP awards, and multiple HST GO awards (GO 12227.001, 12664.001, 12519.001, 14713.001) from the Space Telescope Science Institute.

References

Blackman, E. G., & Lucchini, S. 2014, *MNRAS*, 440, L16
Bujarrabal, V., Castro-Carrizo, A., Alcolea, J., & Sánchez Contreras, C. 2001, *A & A*, 377, 868
Chamandy, L., Frank, A., Blackman, E. G., *et al.* 2018, *MNRAS*, 480, 1898
Lee, C.-F., & Sahai, R. 2004, *ApJ*, 606, 483
Claussen, M.J., Sahai, R., & Morris, M., 2009, ApJ, 691, 219
De Marco, O. 2009, *PASP*, 121, 316
Huang, P.-S. & Sahai, R. 2018, *in prep*
Imai, H. 2007, *Astrophysical Masers and their Environments, IAU Symposium 242*, 242, 279
Ivanova, N., Justham, S., Chen, X., *et al.* 2013, *A & ARv*, 21, 59
Jones, D. 2018, arXiv:1806.08244
Kamath D., Wood P. R. & Van Winckel H. 2015, *MNRAS*, 454, 1468
Kamath D., Wood P. R., Van Winckel H. & Nie J. D. 2016, *A&A*, 586, L5

Kastner, J. H., Montez, R., Jr., Balick, B., *et al.* 2012, *AJ*, 144, 58
Kervella, P., Montargès, M., Lagadec, E., *et al.* 2015, *A & A*, 578, A77
Kervella, P., Homan, W., Richards, A. M. S., *et al.* 2016, *A & A*, 596, A92
Knapp, G. R., Jorissen, A., & Young, K. 1997, *A & A*, 326, 318
Luttermoser, D. G., Johnson, H. R., & Eaton, J. 1994, *ApJ*, 422, 351
Montez, R., Jr., Ramstedt, S., Kastner, J. H., Vlemmings, W., & Sanchez, E. 2017, *ApJ*, 841, 33
Neckel, T., Staude, H. J., Sarcander, M., & Birkle, K. 1987, *A & A*, 175, 231
Nhung, P. T., Hoai, D. T., Diep, P. N., *et al.* 2016, *Research in Astronomy and Astrophysics*, 16, 111
Ortiz, R. & Guerrero, M. 2016, *MNRAS*, 3036, 3046
Sahai, R. 2009, *Asymmetric Planetary Nebulae IV proc., I.A.C. electronic publication, eds. R.L.M. Corradi, A. Manchado & N. Soker*, http://www.iac.es/proyecto/apn4/pages/proceedings.php
Sahai. R., Findeisen, K., Gil de Paz, A., Sáanchez Contreras, C. 2008, ApJ, 689, 1274 [Setal08]
Sahai, R., Le Mignant, D., Sánchez Contreras, C., Campbell, R. D., Chaffee, F. H. 2005, ApJ, 622, L53
Sahai, R., Morris, M. R., & Villar, G. G. 2011a, *A&A*, 141, 134
Sahai, R., Morris, M., Knapp, G.R., Young, K., Barnbaum, C. 2003, *Nature*, 426, 261
Sahai, R., Morris, M., Sánchez Contreras, C., & Claussen, M. 2007, *AJ*, 134, 2200
Sahai, R., Neill, J. D., Gil de Paz, A., & Sánchez Contreras, C. 2011b, *ApJ Let*, 740, L39
Sahai, R. & Nyman, L-Å. 1997, ApJ, 487, L155
Sahai, R., Sanz-Forcada, J., & Sánchez Contreras, C. 2016a, *Journal of Physics Conf. Ser.*, 728, 042003
Sahai, R., Scibelli, S., & Morris, M. 2016b, *ApJ*, 827, 92
Sahai, R., Sugerman, Ben, E.K., Hinkle, K. 2009, *ApJ*, 699, 1015
Sahai, R., Sanz-Forcada, J., Sánchez Contreras, C., & Stute, M. 2015, ApJ, 810, 77 [Setal15]
Sahai, R., Te Lintel Hekkert, P., Morris, M., Zijlstra, A., Likkel, L. 1999, ApJ, 514, L115
Sahai, R. & Trauger, J.T. 1998, *AJ*, 116, 1357
Sahai, R., Vlemmings, W. H. T., Gledhill, T., *et al.* 2017a, *ApJ Let*, 835, L13 [Setal17]
Sahai R., Vlemmings W. H. T., Huggins P. J., *et al.* 2013, *ApJ*, 777, 92
Sahai, R., Vlemmings, W. H. T., & Nyman, L.-Å. 2017b, *ApJ*, 841, 110
Sahai, R., Young, K., Patel, N. A., Sánchez Contreras, C., & Morris, M. 2006, *ApJ*, 653, 1241
Sahai, R., Sánchez Contreras, C., Mangan, A. S., *et al.* 2018a, *ApJ*, 860, 105 [Setal18]
Sahai, R., Rajagopal, J., Hinkle, K., Joyce, R. & Morris, M. 2018b, this volume
Sahai, R. 2018a, arXiv:1810.06685
Sahai, R. 2018b, Galaxies, 6, 102
Sánchez Contreras, C., Bujarrabal, V., Castro-Carrizo, A., Alcolea, J., & Sargent, A. 2006, *ApJ*, 643, 945
Scibelli, S., Sahai, R., & Morris, M. 2018, *ApJ*, submitted
Snaid, S., Zijlstra, A. A., McDonald, I., *et al.* 2018, *MNRAS*, 477, 4200
Soker, N. 2015, *ApJ*, 800, 114

https://doi.org/10.1017/S1743921319001819 Published online by Cambridge University Press